Coherence-based Beamforming algorithm for vehicle cabin acoustic comfort evaluation

Francesco Uffreduzzi[a]* | Alessandro Aquili[a] | Raj Mattias Mehta[a]

[a] Pininfarina SpA,
Via Nazionale, 30, 10020 Cambiano (TO)
* Corresponding author:
f.uffreduzzi@pininfarina.it

Ricevuto: 13/3/2024
Accettato: 10/5/2024

DOI: 10.3280/ria1-2024oa17464
ISSNe: 2385-2615

The growing importance of electric vehicles in the global market makes the reduction of wind noise a crucial point for investing money and resources. To improve vehicle acoustic comfort, it is increasingly important to identify aeroacoustic noise sources around the vehicle, many of which were previously masked by engine noise. The Beamforming techniques are widely used methods that, thanks to one or more arrays of microphones, localize the noise sources on a virtual plane close to the object. However, not all the sources highlighted infiltrate the vehicle cabin and affect its acoustic comfort. Based on these considerations, the Pininfarina Wind Tunnel developed an algorithm capable of correlating the various sound sources detected by the Conventional Beamforming technique to the noise measured inside the vehicle cabin. Unlike conventional approaches, this so-called Coherence Beamforming algorithm was successfully able to remove the uncorrelated aerodynamic noise contributions, isolating the major noise sources responsible for passenger discomfort.
Keywords: acoustic comfort, aeroacoustics, automotive, coherence beamforming, microphone array, wind tunnel

Algoritmo di Beamforming coerente per la valutazione del comfort acustico interno di un veicolo
La crescente importanza dei veicoli elettrici nel mercato globale rende la riduzione del rumore aerodinamico un argomento cruciale su cui investire denaro e risorse. Per migliorare il comfort acustico di un'automobile è ora più che mai necessario identificare correttamente le sorgenti sonore aeroacustiche attorno al veicolo, molte delle quali in precedenza mascherate dal rumore del motore. Le tecniche di Beamforming sono generalmente utilizzate per localizzare le sorgenti di rumore su un piano virtuale in prossimità di un oggetto, elaborando i segnali acquisiti da uno o più array di microfoni. Non tutte le sorgenti rilevate, però, sono in grado di raggiungere l'abitacolo dell'auto e di influenzarne il comfort acustico. Sulla base di queste considerazioni, la galleria del vento Pininfarina ha sviluppato un algoritmo in grado di correlare le varie sorgenti aeroacustiche identificate dalla tecnica di Beamforming Convenzionale con il rumore misurato all'interno dell'auto. A differenza degli approcci convenzionali, il cosiddetto algoritmo di Beamforming Coerente ha rimosso con successo il contributo del rumore aerodinamico non coerente, isolando le principali sorgenti in grado di influire negativamente sul comfort dei passeggeri.
Parole chiave: comfort acustico, aeroacustica, automotive, Beamforming coerente, array di microfoni, galleria del vento

1 | Introduction

The automotive industry has greatly benefited from the improvements in microphone array techniques over the last two decades. The most common wind tunnel application for wind noise investigation is the use of out-of-flow planar beamforming arrays to localize and quantify exterior aeroacoustic noise sources such as side-view mirror, A-pillar, wheelhouse arch etc. [1–3].

Through continuous development, the sound maps of today are significantly more detailed than previous methods: dynamic and spatial resolution of acoustic maps has been improved thanks to the introduction of optimized geometries of arrays [4] and with the formulation of deconvolution algorithms such as DAMAS, CLEAN, CLEAN-SC etc. [5,6]. Nevertheless, classical Beamforming formulations cannot evaluate the real impact of exterior noise sources on interior noise level.

Beamforming using a spherical array of microphones installed inside the car cabin allows for the identification of the areas that contribute most to the interior noise level [7]. However, this characterization is not sufficiently accurate to localize the exterior aeroacoustic sources responsible for these emissions.

To overcome these limitations, several approaches have been introduced to determine the contribution of exterior aeroacoustic sources on interior noise [8-11]. The purpose of the present work, itself an extension of previous research [12], was to develop an algorithm capable of identifying the aeroacoustic sources that penetrate the cabin and impact passenger comfort. This was achieved by correlating external array signals with an additional microphone installed inside the vehicle.

Copyright © FrancoAngeli.
This work is released under Creative Commons Attribution - Non-Commercial – No Derivatives License.
For terms and conditions of usage please see:
http://creativecommons.org.

2 | Coherence Beamforming

2.1 | Pininfarina wind tunnel facility

Since 2005, Pininfarina has utilized a Beamforming system based on microphone arrays to investigate the external noise sources of vehicles in the full-scale wind tunnel. This system identifies noise sources in a virtual plane close to the vehicle and parallel to the one on which the microphones lie. The wind tunnel is equipped with:

- An overhead array (Fig. 1), located on the ceiling of the test section (4 m from the floor), which consists of 78 Brüel & Kjær Type 4951 microphones whose specifications are reported in Tab. 1.
- A lateral array (Fig. 1), placed on the side wall of the test section, with 66 Brüel & Kjær Type 4951 microphones whose characteristics are the same already introduced in Tab. 1.
- A smaller frontal array (Fig. 2), installed above the nozzle exit, with 15 Brüel & Kjær Type 4189 microphones whose specifications are summarized in Tab. 2.

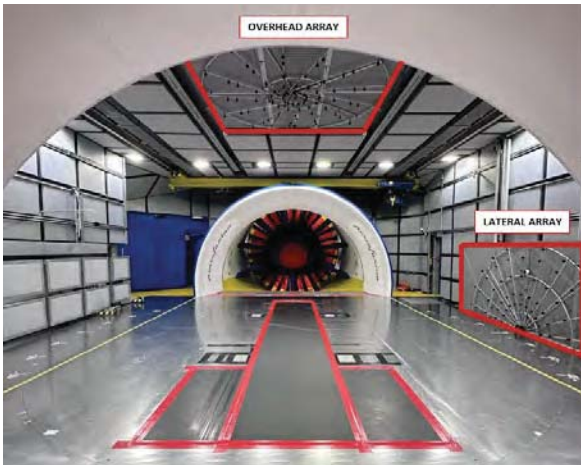

Fig. 1 – Pininfarina side and overhead arrays
Array laterale e superiore Pininfarina

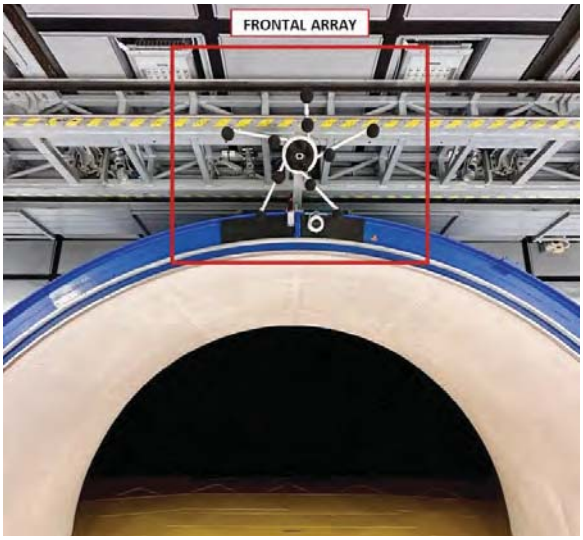

Fig. 2 – Pininfarina frontal array
Array frontale Pininfarina

Tab. 1 – Brüel & Kjær 4951 specifications
Specifiche Brüel & Kjær 4951

Sensitivity	6.3 mV/Pa
Frequency	100 Hz – 20 kHz
Dynamic Range	35 – 140 dB
Temperature	–10 °C to +55 °C
Polarization	prepolarized

Tab. 2 – Brüel & Kjær 4189 specifications
Specifiche Brüel & Kjær 4189

Sensitivity	50 mV/Pa
Frequency	6.3 Hz – 20 kHz
Dynamic Range	14.6 – 146 dB
Temperature	–30 °C to +150 °C
Polarization	prepolarized

2.2 | Algorithm

The Pininfarina Conventional Beamforming algorithm is based on the cross-spectral imaging function, deeply described in [13]. The Coherence Beamforming technique introduced here takes inspiration from [14] and makes use of an additional reference microphone recorded synchronously with the external arrays. The coherent beamformer power output requires the computation of a cross-spectral matrix defined, for a single frequency and a single microphone, as follows:

$$\boldsymbol{C_{xy}(i_{Mik}, f)} = \frac{1}{N_w}\sum_{k=1}^{N_w} \boldsymbol{P_{i_{Mik}}(f) P_{Ref}(f)^*} \tag{1}$$

where $P_{iMik}(f)$ is the two-sided Fast Fourier Transform (FFT) of the i^{th} microphone, P_{Ref} is the two-sided FFT of the reference microphone and the symbol (.)* stands for the complex-conjugate operator. The single-sided form of the cross spectral matrix is then obtained by multiplying each frequency by two and discarding the second half of the array. This formulation leads to an output influenced by the arrays' signals, tending to amplify the coherent beamformer power output inside the cabin when there is high coherence between the internal recorded signal and the external ones. To avoid this, the cross spectral matrix has been rescaled as follows:

$$\overline{\boldsymbol{C_{xy}(i_{Mik}, f)}} = \frac{1}{N_w}\sum_{k=1}^{N_w} \boldsymbol{2 \cdot \frac{P_{iMik}(f) P_{Ref}(f)^*}{\sqrt{P_{i_{Mik}\, i_{Mik}}(f)}}} \tag{2}$$

where $P_{iMik\, iMik}$ is the i^{th} microphone average power spectrum computed as:

$$\boldsymbol{P_{i_{Mik}\, i_{Mik}}(f)} = \frac{1}{N_w}\sum_{k=1}^{N_w} \boldsymbol{P_{i_{Mik}}(f) P_{i_{Mik}}(f)^*} \tag{3}$$

The coherent beamformer power output, for a single grid point x_G and a single frequency f, is then obtain from:

$$\boldsymbol{P_{Coh}(x_G, f)} = \frac{1}{N_{Miks}}\sum_{i_{Mik}=1}^{N_{Miks}} \overline{\boldsymbol{C_{xy}}}\, \boldsymbol{e^{j2\pi f \frac{d_{iMik}}{c}}} \tag{4}$$

Copyright © FrancoAngeli.
This work is released under Creative Commons Attribution - Non-Commercial – No Derivatives License.
For terms and conditions of usage please see:
http://creativecommons.org.

where d_{iMik} is the distance of the i^{th} microphone from the grid point x_G, c is the speed of sound and $\overline{C_{xy}} = \overline{C_{xy}(i_{Mik}, f)}$ is the rescaled cross spectral matrix defined in Eq. (2).

A validation campaign was performed to assess the validity of this new methodology prior to its use during the wind tunnel sessions. The following paragraphs present the most important results obtained from the testing campaign. A real test case on a production car will be also introduced to show the advantages of using this formulation.

3 | Validation campaign

3.1 | Experimental set-up

The validation campaign was performed using a Brüel & Kjær Omnisource Sound Source Type 4295. The size and shape of its orifice have been carefully engineered to radiate sound evenly in all directions. Thus, Type 4295 fulfils the national and international standards for omnidirectional sound sources, as reported in Fig. 3 and Fig. 4.

The experimental set-up, shown in Fig. 5 and Fig. 6, was arranged in order to replicate real automotive test conditions (in terms of distances between the source and the arrays).

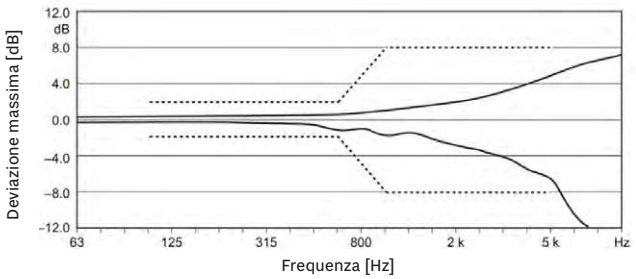

Fig. 3 – Maximum allowed directional deviation of an omnidirectional sound source according to ISO 140 (averaged over 'gliding' 30° arcs in a free sound field). Upper and lower dotted curves are the ISO tolerances

Deviazione direzionale massima consentita rispetto ad una sorgente omnidirezionale in accordo con la ISO 140 (media su archi di 30° in campo sonoro libero). Le curve tratteggiate superiore e inferiore sono le tolleranze della normativa ISO

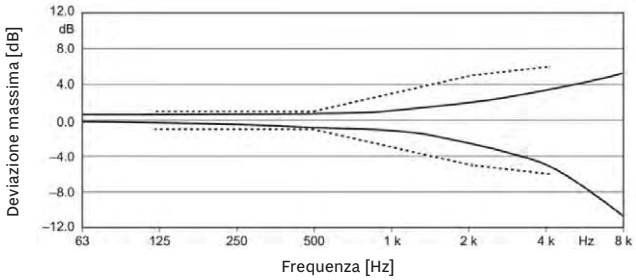

Fig. 4 – Maximum allowed directional deviation of an omnidirectional sound source according to ISO 3382-1 (averaged over 'gliding' 30° arcs in a free sound field). Upper and lower dotted curves are the ISO tolerances

Deviazione direzionale massima consentita rispetto ad una sorgente omnidirezionale in accordo con la ISO 3382-1 (media su archi di 30° in campo sonoro libero). Le curve tratteggiate superiore e inferiore sono le tolleranze della normativa ISO

For the first test, the Brüel & Kjær Omnisource Sound Source Type 4295 was placed at 3 m from the centre of the side array and at 2.8 m from the overhead array.

The second test assessed the performance of the frontal array. In this case, the Brüel & Kjær Omnisource Sound Source Type 4295 was positioned at 2.4 m from it.

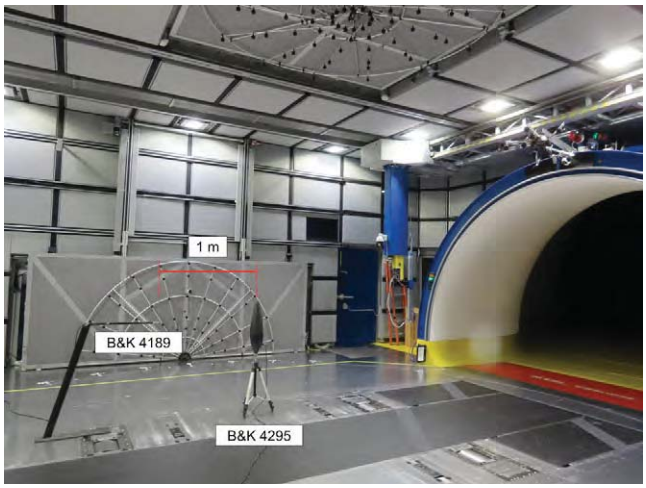

Fig. 5 – Side and overhead array validation test case experimental set-up

Set-up sperimentale per il caso di validazione dell'array laterale e superiore

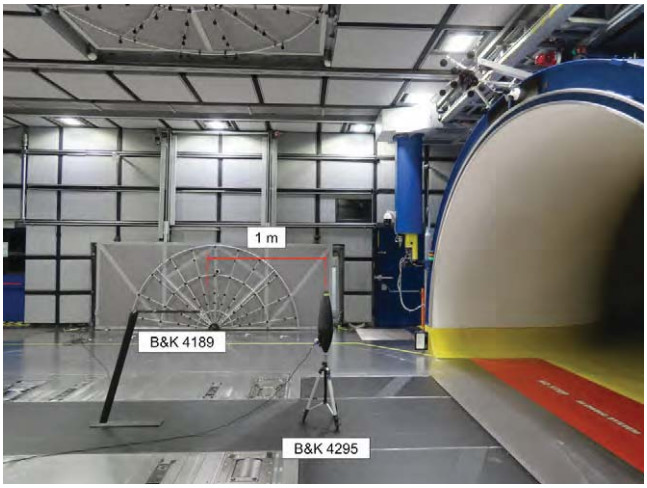

Fig. 6 – Frontal array validation test case experimental set-up

Set-up sperimentale per il caso di validazione dell'array frontale

In both cases, a Brüel & Kjær 4189 free field reference microphone was positioned at 1 m from the source. The microphone specifications are the same already introduced in Tab. 2 and its typical free field response is depicted in Fig. 7.

Copyright © FrancoAngeli.
This work is released under Creative Commons Attribution - Non-Commercial – No Derivatives License.
For terms and conditions of usage please see:
http://creativecommons.org.

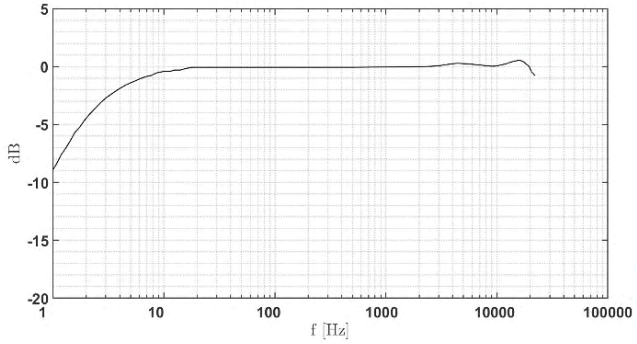

Fig. 7 – Typical free-field response of Brüel & Kjær 4189 microphone with protection grid

Tipica risposta in campo libero del microfono Brüel & Kjær 4189 con griglia di protezione

3.2 | Results

In order to validate the algorithm, a white noise signal was used. The reference microphone was synchronously acquired along with the arrays' receivers, considering an acquisition time T = 6.25 s and a sampling frequency f_s = 32768 Hz. The frequency range of interest span from 250 Hz to 5000 Hz.

Fig. 8 shows a comparison between the source Sound Pressure Level (SPL) measured by the reference microphone and the one obtained through the Conventional and Coherence Beamforming algorithm, for all the three arrays. All the arrays' spectra are calculated at 1 m from the source. The curves retrieved by the two Beamforming algorithms are plotted considering the maximum SPL value obtained on the zone of interest for each frequency.

As seen in Fig. 8, all the curves are in good agreement over the whole frequency range and the Coherence Beamforming algorithm results closely follow the reference microphone SPL for all the three arrays.

Focusing on the sound maps, the Coherence Beamforming algorithm results match the conventional methodology in terms of source localization, providing slightly different SPL values since the arrays signals are statistically conditioned by the correlations with the reference microphone.

Examples of sound maps obtained with the two different algorithms for the one-third octave band centered at f = 2500 Hz are reported in Fig. 9, Fig. 10 and Fig. 11.

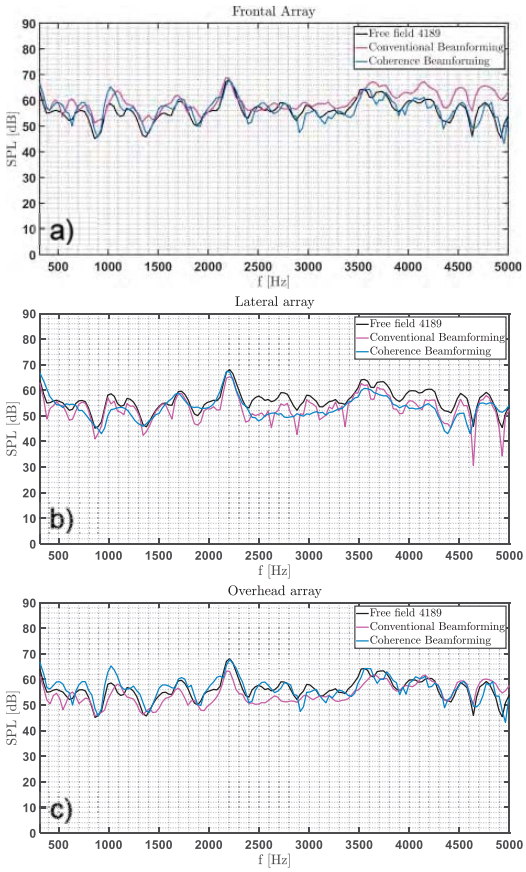

Fig. 8 – SPL at 1 m from the source. Conventional and Coherence Beamforming algorithm vs reference microphone for frontal (a), lateral (b) and overhead array (c)

Livello di pressione sonora a 1 m dalla sorgente. Beamforming Convenzionale e Coerente vs microfono di riferimento per l'array frontale (a), laterale (b) e superiore (c)

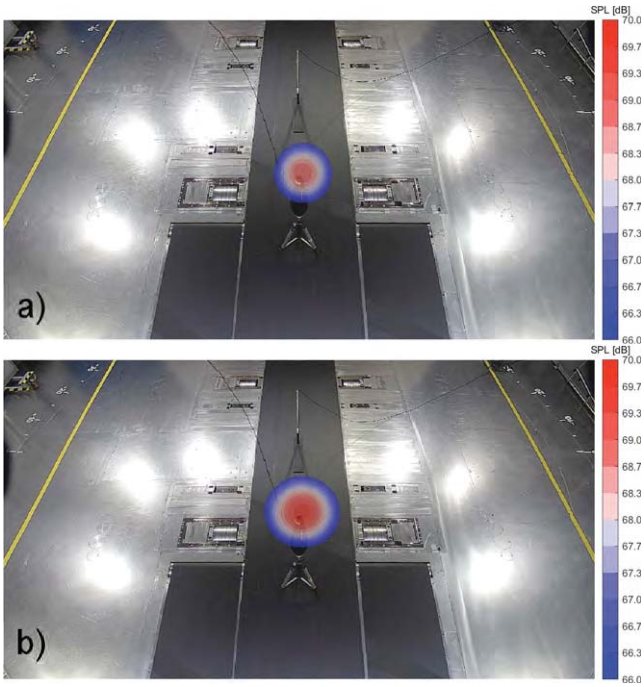

Fig. 9 – Frontal array conventional (a) vs coherent (b) sound map for the 2500 Hz one-third octave band

Mappa acustica convenzionale (a) e coerente (b) dell'array frontale per il terzo di ottava 2500 Hz

Copyright © FrancoAngeli.
This work is released under Creative Commons Attribution - Non-Commercial – No Derivatives License.
For terms and conditions of usage please see:
http://creativecommons.org.

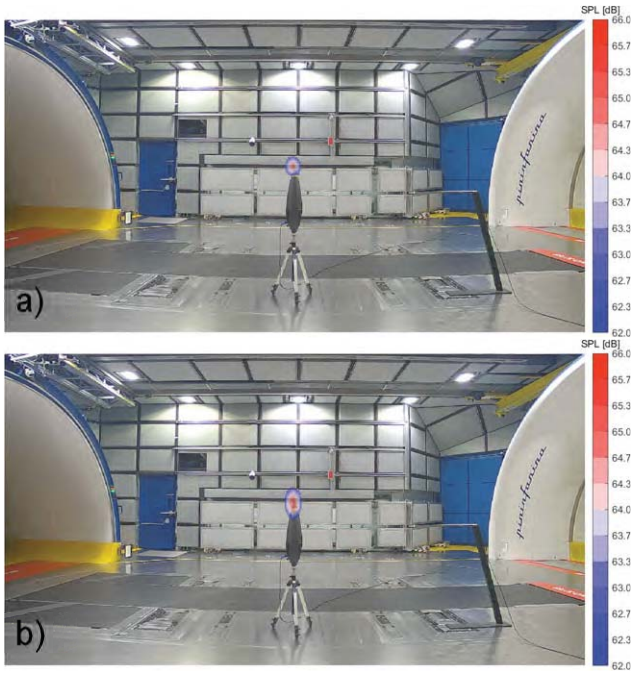

Fig. 10 – Lateral array conventional (a) and coherent (b) sound map for the 2500 Hz one-third octave band

Mappa acustica convenzionale (a) e coerente (b) dell'array laterale per il terzo di ottava 2500 Hz

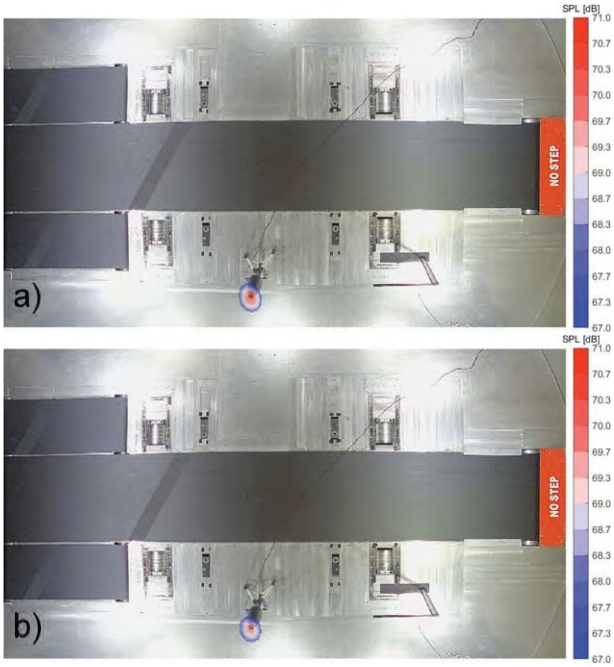

Fig. 11 – Overhead array conventional (a) vs coherent (b) sound map for the 2500 Hz one-third octave band

Mappa acustica convenzionale (a) e coerente (b) dell'array superiore per il terzo di ottava 2500 Hz

4 | Real case

4.1 | Experimental set-up

For the real case, all the measurements were performed on a production car at various wind speeds. The vehicle was placed inside the test section ensuring its alignment with the streamwise centreline of the wind tunnel, following the standard set-up used for aeroacoustic investigations. This requires testing the car with stationary wheels and floor. While these conditions are typically crucial to the proper simulation of vehicle aerodynamic behaviour, the noise generated by the Wheel Drive Units (WDU) and the moving belt system compromise aeroacoustic characterization by increasing background noise and creating non-aeroacoustic noise sources.

A Brüel & Kjær diffuse field 4942 microphone was installed inside the car, at the same position as the driver's head, oriented towards the side-view mirror (Fig. 12). In addition, a KingState KPE-141 source was placed as highlighted in Fig. 13. The tonal noise frequency emitted by this source was set to 3850 Hz.

The diffuse field microphone has the specifications reported in Tab. 3 and its typical random-incidence response is depicted in Fig. 14.

Fig. 12 – Diffuse field microphone installation inside the car

Installazione microfono a campo diffuso all'interno della vettura

Fig. 13 – KingState KPE-141 noise generator installation

Installazione della sorgente acustica KingState LPE-141

Tab. 3 – Brüel & Kjær 4942 specifications

Specifiche Brüel & Kjær 4942

Sensitivity	50 mV/Pa
Frequency	6.3 Hz – 16 kHz
Dynamic Range	14.6 – 146 dB
Temperature	–40 °C to +150 °C
Polarization	0 V

Copyright © FrancoAngeli.
This work is released under Creative Commons Attribution - Non-Commercial – No Derivatives License.
For terms and conditions of usage please see:
http://creativecommons.org.

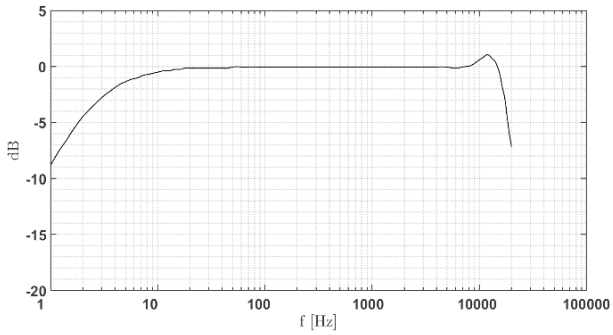

Fig. 14 – Typical diffuse-field response of Brüel & Kjær 4942 microphone with protection grid

Tipica risposta in campo diffuso del microfono Brüel & Kjær 4942 con griglia di protezione

The most important results obtained by testing the vehicle at various flow speeds will be presented in the following paragraphs. The initial focus will be on the frontal and overhead arrays, then the performance of the side array will be analysed. The frequency range of interest was set between 250 Hz and 5000 Hz.

4.2 | Results

4.2.1 | V=60 km/h

Fig. 15 shows a comparison between the SPL measured by the reference microphone and the one obtained through the Conventional and Coherence Beamforming algorithm applied to all the three arrays. For the case presented in this study, the various array spectra have been calculated at the array plane. Due to its small diameter, the frontal array lower cut-off frequency is 1000 Hz.

In the new algorithm, a peak is found whenever there is a high level of coherence between the external receivers and the internal one. This means that the noise measured by the external arrays is able to pass inside the vehicle cabin. On the contrary, when there is minimal correlation between the signals, the resulting SPL values are very low or even negative.

The lowest frequency peak, visible from the overhead array Coherence Beamforming spectrum (Fig. 15c), occurs at f = 480 Hz and is due to a noise source located in the rear part of the vehicle, as depicted in Fig. 16. At first glance, noise could be attributed to the main fan, which is close to the rear of the vehicle. However, the following investigations proved that it came from the trunk:

- A subjective evaluation was used to localize the low frequency noise in the trunk area.
- A parametric investigation, moving the car forward by 400 mm, resulted in a source shift which followed the vehicle displacement (see Fig. 17).

By combining the information from the external and internal measurements, the Coherence Beamforming algorithm was able to highlight a noise source that was hidden when the signals were analysed separately. When looking at the Conventional Beamforming output or the reference microphone spectra, the source was masked by background noise, with only a slight peak noticeable.

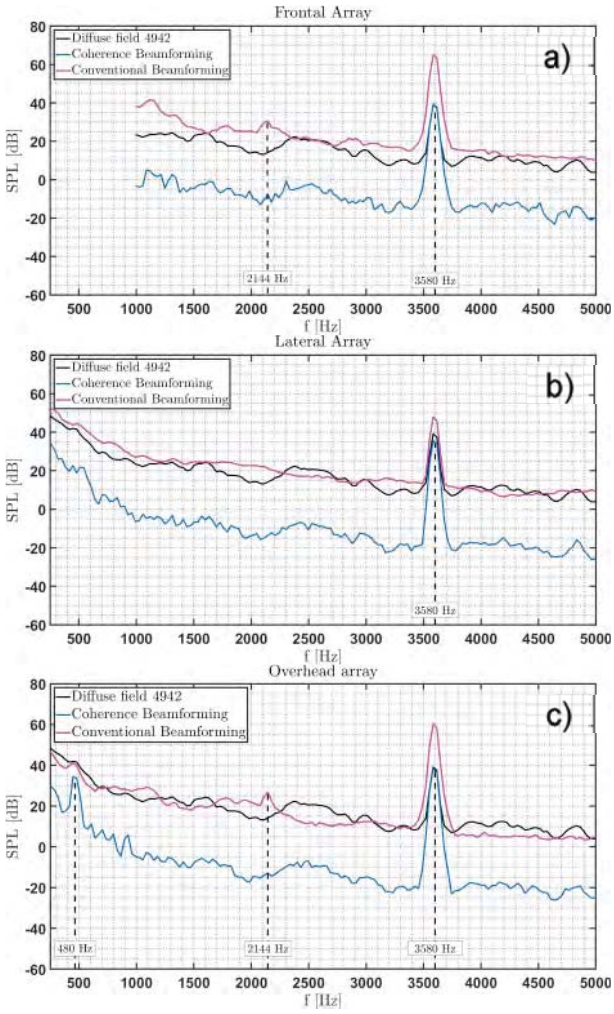

Fig. 15 – SPL at V=60 km/h. Conventional and Coherence Beamforming algorithm vs reference microphone for frontal (a), lateral (b) and overhead array (c)

Livello di pressione sonora a V=60 km/h. Beamforming Convenzionale e Coerente vs microfono di riferimento per l'array frontale (a), laterale (b) e superiore (c)

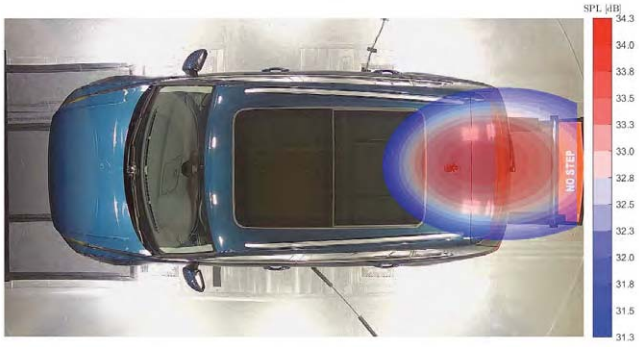

Fig. 16 – Overhead array coherent sound map for the 500 Hz one-third octave band

Mappa acustica coerente dell'array superiore per il terzo di ottava 500 Hz

Copyright © FrancoAngeli.
This work is released under Creative Commons Attribution - Non-Commercial – No Derivatives License.
For terms and conditions of usage please see:
http://creativecommons.org.

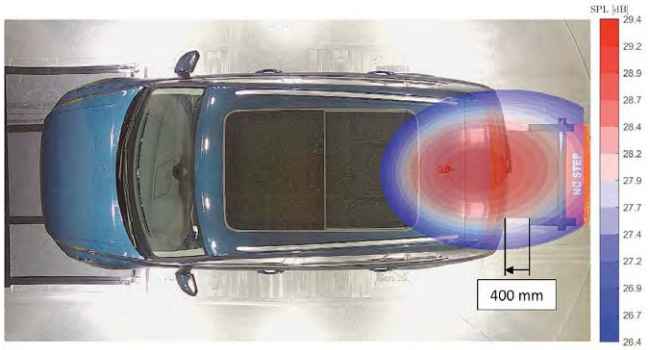

Fig. 17 – Overhead array coherent sound map for the 500 Hz one-third octave band. Car shifted 400 mm forward

Mappa acustica coerente dell'array superiore per il terzo di ottava 500 Hz. Vettura spostata 400 mm in Avanti

A second peak can be seen at f = 2144 Hz, for both the frontal and the overhead array (Fig. 15a, Fig. 15c), but only in the Conventional Beamforming integrated spectra and not in the Coherence Beamforming ones. This tonal emission is produced by the vehicle front grille and is only perceived from outside.

Fig. 18 and Fig. 19 show a comparison between the sound maps obtained using the two algorithms in the frequency range 2050-2250 Hz. While the Conventional Beamforming precisely localizes the noise source, the Coherence Beamforming fails due to a low level of correlation between the external receivers and the internal reference one. This is also evident by looking at the very low SPL values obtained from the maps.

Finally, as depicted in Fig. 20, the tonal noise emitted by the synthetic source is precisely detected by all three microphone arrays and also perceived inside the vehicle cabin.

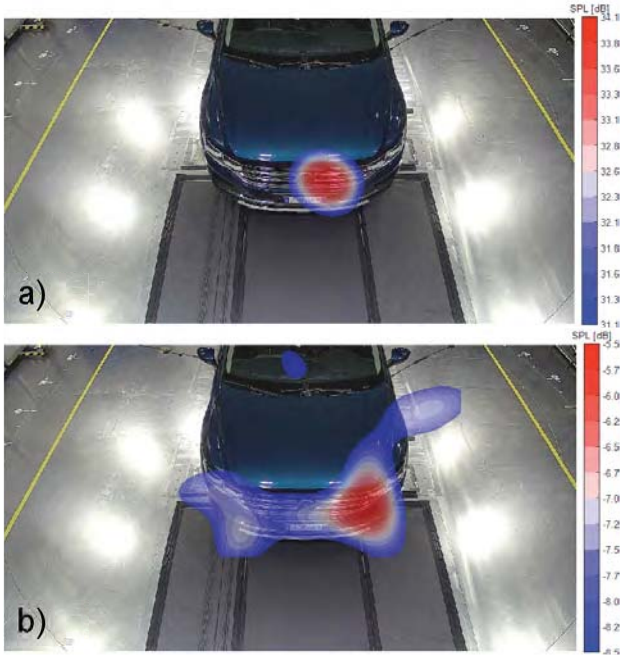

Fig. 18 – Frontal array conventional (a) and coherent (b) sound map in the frequency range 2050-2250 Hz

Mappa acustica convenzionale (a) e coerente (b) dell'array frontale nel range di frequenza 2050-2250 Hz

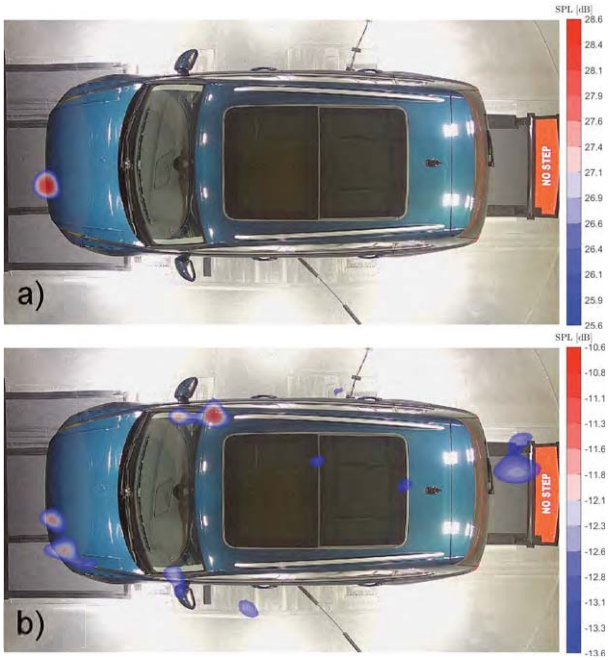

Fig. 19 – Overhead array conventional (a) and coherent (b) sound map in the frequency range 2050-2250 Hz

Mappa acustica convenzionale (a) e coerente (b) dell'array superiore nel range di frequenza 2050-2250 Hz

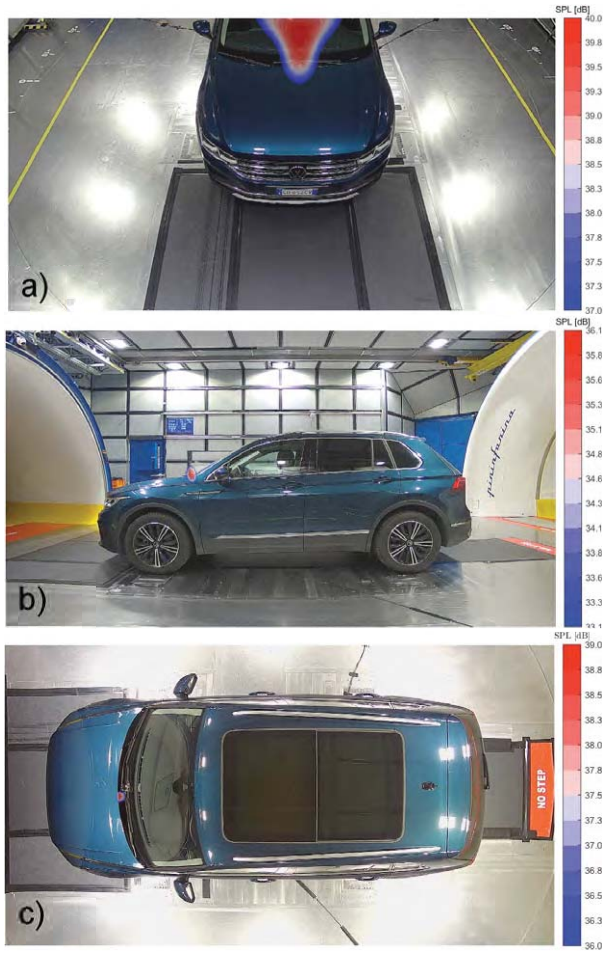

Fig. 20 – Frontal (a), lateral (b) and overhead (c) array coherent sound map for the 4000 Hz one-third octave band

Mappa acustica coerente dell'array frontale (a), laterale (b) e superiore (c) per il terzo di ottava 4000 Hz

Copyright © FrancoAngeli.
This work is released under Creative Commons Attribution - Non-Commercial – No Derivatives License.
For terms and conditions of usage please see:
http://creativecommons.org.

Consequently, the Coherence Beamforming spectra show SPL values very close to the ones measured by the reference microphone (as evident in Fig. 15). For this specific case, the lateral array sound map, which is usually computed on a plane cutting the vehicle left side-view mirror (generally at 3.4 m from the array), has been evaluated at 4.2 m, equivalent to the distance between the array and the synthetic source.

4.2.2 | V=100 km/h

As the wind tunnel flow speed is increased, a new peak can be found in the Coherence Beamforming SPL integrated spectra, as shown in Fig. 21. The vehicle front grille produces a tonal noise at f = 2368 Hz which is heard both from outside and inside the car cabin and can be seen in the Coherence Beamforming third-octave sound maps reported in Fig. 22.

The overhead array Coherence Beamforming spectrum also reveals three lower peaks in the 600-1000 Hz frequency range that can be ascribed to a flow interaction with the left

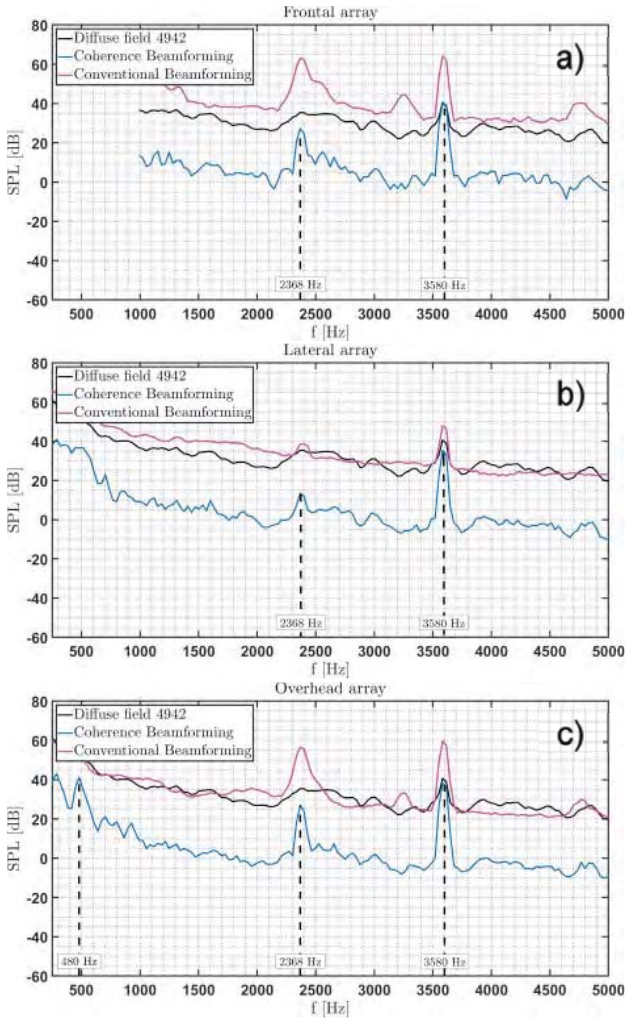

Fig. 21 – SPL at V=100 km/h. Conventional and Coherence Beamforming algorithm vs reference microphone for frontal (a), lateral (b) and overhead (c) array

Livello di pressione sonora a V=100 km/h. Beamforming Convenzionale e Coerente vs microfono di riferimento per l'array frontale (a), laterale (b) e superiore (c)

Fig. 22 – Frontal (a), lateral (b) and overhead (c) array coherent sound map for the 2500 Hz one-third octave band

Mappa acustica coerente dell'array frontale (a), laterale (b) e superiore (b) per il terzo di ottava 2500 Hz

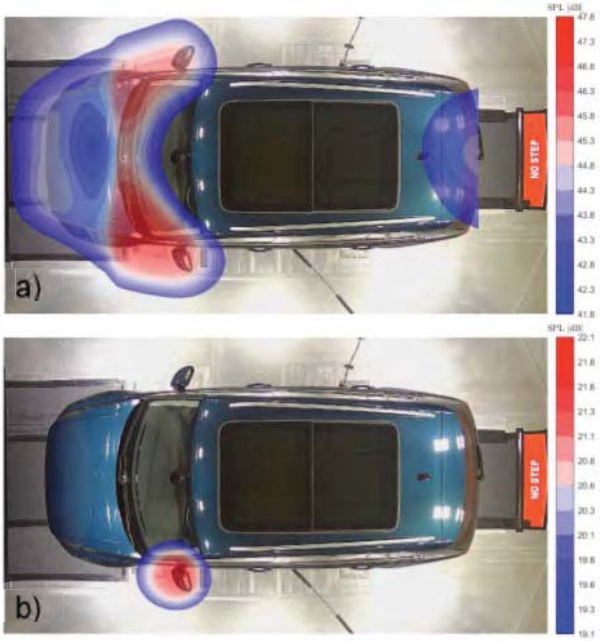

Fig. 23 – Conventional Beamforming (a) vs Coherence Beamforming (b) for the 800 Hz one-third octave band

Beamforming Convenzionale (a) vs Beamforming Coerente (b) per il terzo di ottava 800 Hz

Copyright © FrancoAngeli.
This work is released under Creative Commons Attribution - Non-Commercial – No Derivatives License.
For terms and conditions of usage please see:
http://creativecommons.org.

side-view mirror. By performing the coherence between the signals acquired by the array and the internal microphone, only the noise emitted by this sound source shows high level of correlation.

Fig. 23 shows a comparison between the sound map obtained through the Conventional Beamforming algorithm and the one obtained through the Coherence Beamforming for the one-third octave band centered at f = 800 Hz. As can be seen, the Conventional Beamforming tends to adequately localize the noise sources around the windshield and the front of the car, while the Coherence Beamforming precisely localizes the origin of the noise on the left side-view mirror.

5 | Conclusions

This work proposes the implementation and application of Coherence based Beamforming in the frame of an automotive aeroacoustic wind tunnel testing. The method was compared with a Conventional Beamforming algorithm using a known noise source, as well as on a real vehicle. Conventional Beamforming clearly identifies the location of major sound sources but fails if low intensity sound sources are masked by louder ones or by broadband frequency noise. The Coherence method utilizes a reference signal so as to denoise the microphone arrays. This removes the uncorrelated aerodynamic noise contribution in order to determine the impact of outside sources on the interior noise. The outputs of the Coherence based Beamforming technique successfully identify the major noise sources responsible for passenger discomfort, otherwise unrecognized with conventional approaches.

Since the acoustic maps are computed on a single plane close to the vehicle, they may slightly misrepresent the intensity and location of the out-of-plane noise sources, especially for the overhead array. To improve the results of the Beamforming techniques, these maps could be calculated on a topology more representative of the vehicle shape. As a first approach, Pininfarina is already using a multi-plane formulation for the overhead array. This involves the definition of several planes that better describe the height variation of the vehicle. The natural evolution of the multi-plane approach is to directly map the noise sources on a 3D scan of the car. While this method has been successfully used in research applications, it is not still compatible with Pininfarina's testing procedure due to the amount of time required to obtain the vehicle scan. Future research studies will be focused on streamlining this process to minimize its impact on testing time. Due to the large 3D domain, a deconvolution method like CLEAN-SC could be beneficial and will also be explored.

Conclusioni

Questo studio propone l'implementazione e l'applicazione di un algoritmo di Beamforming basato sulla coerenza nell'ambito di test aeroacustici in una galleria del vento automotive. Il metodo è stato confrontato con un algoritmo di Beamforming Convenzionale, utilizzando prima una sorgente di rumore nota e poi facendo dei test su una vettura di produzione. Il Beamforming Convenzionale identifica chiaramente la posizione delle principali sorgenti sonore, ma fallisce se quelle a bassa intensità sono mascherate da sorgenti più intense o da un rumore a banda larga. Il metodo qui introdotto utilizza un segnale di riferimento per depurare le misure degli array di microfoni. In tal modo è possibile rimuovere il contributo del rumore aerodinamico non coerente per determinare l'impatto delle sorgenti esterne sul rumore interno. I risultati del Beamforming basato sulla coerenza evidenziano con successo le principali fonti di rumore capaci di influire sul comfort dei passeggeri, altrimenti non identificabili con gli approcci convenzionali.

Le mappe acustiche sono calcolate su un singolo piano in prossimità del veicolo, pertanto possono rappresentare in modo non del tutto esatto l'intensità e la posizione delle sorgenti di rumore giacenti al di fuori di esso, soprattutto nel caso dell'array superiore. Per migliorare i risultati delle tecniche di Beamforming, tali mappe potrebbero essere calcolate su una topologia più rappresentativa della forma del veicolo. Attualmente, in Pininfarina è in uso una formulazione multi-piano associata all'array superiore. Ciò permette la definizione di diversi piani in grado di descrivere meglio la variazione di altezza del veicolo. La naturale evoluzione dell'approccio multi-piano consiste nel mappare direttamente le sorgenti di rumore su una scansione 3D dell'auto. Sebbene questo metodo sia stato utilizzato con successo in varie attività di ricerca, non è ancora compatibile con la procedura di test adottata da Pininfarina a causa del tempo richiesto per realizzare le scansioni tridimensionali. I futuri studi si concentreranno sulla semplificazione di questo processo per ridurne l'impatto sui tempi di prova. A causa delle estese dimensioni del dominio 3D, un metodo di deconvoluzione come il CLEAN-SC potrebbe essere utile e verrà dunque esplorato.

Bibliography

[1] K.-H. Chen, J. Johnson, U. Dietschi, B. Khalighi, Automotive Mirror Wind Noise Simulations and Wind Tunnel Measurements, in: 14th AIAA/CEAS Aeroacoustics Conference (29th AIAA Aeroacoustics Conference), American Institute of Aeronautics and Astronautics, Vancouver, British Columbia, Canada, 2008. https://doi.org/10.2514/6.2008-2906.

[2] L. Li, J. Li, B. Lu, Y. Liu, Z. Zhang, H. Cheng, Y. Zhang, H. Hou, Application of Beamforming to Side Mirror Aeroacoustic Noise Optimization, in: 2016: pp. 2016-01-0475. https://doi.org/10.4271/2016-01-0475.

[3] D. Lepley, S. Senthooran, D. Hendriana, T. Frazer, Numerical Simulations and Measurements of Mirror-Induced Wind Noise, SAE Int. J. Passeng. Cars – Mech. Syst. 2 (2009) 1550-1562. https://doi.org/10.4271/2009-01-2236.

[4] C.S. Allen, W.K. Blake, R.P. Dougherty, D. Lynch, P.T. Soderman, J.R. Underbrink, Aeroacoustic Measurements, Springer Berlin Heidelberg, Berlin, Heidelberg, 2002. https://doi.org/10.1007/978-3-662-05058-3.

[5] L. de Santana, Fundamentals of Acoustic Beamforming, (n.d.).

[6] Z. Chu, Y. Yang, Comparison of deconvolution methods for the visualization of acoustic sources based on cross-spectral imaging function beamforming, Mechanical Systems and Signal Processing 48 (2014) 404-422. https://doi.org/10.1016/j.ymssp.2014.03.012.

Copyright © FrancoAngeli.
This work is released under Creative Commons Attribution - Non-Commercial – No Derivatives License.
For terms and conditions of usage please see:
http://creativecommons.org.

[7] J. Hald, Spherical Beamforming with Enhanced Dynamic Range, SAE Int. J. Passeng. Cars – Mech. Syst. 6 (2013) 1334-1341. https://doi.org/10.4271/2013-01-1977.

[8] Y. He, B. Wang, Z. Shen, Z. Yang, G. Heilmann, T. Zhang, G. Dong, Correlation Analysis of Interior and Exterior Wind Noise Sources of a Production Car Using Beamforming Techniques, in: 2017: pp. 2017-01–0449. https://doi.org/10.4271/2017-01-0449.

[9] J. Hald, H. Kuroda, T. Makihara, Y. Ishii, Mapping of contributions from car-exterior aerodynamic sources to an in-cabin reference signal using Clean-SC, (2016).

[10] J.-L. Adam, D. Ricot, C. Lambourg, A. Menoret, Correlated Beamforming Method for Relevant Aeroacoustic Sources Identification, in: 2009: pp. 2009-01-2234. https://doi.org/10.4271/2009-01-2234.

[11] S. Guidati, R. Sottek, Advanced Source Localization Techniques Using Microphone Arrays, SAE Int. J. Passeng. Cars – Mech. Syst. 4 (2011) 1241-1249. https://doi.org/10.4271/2011-01-1657.

[12] F. Uffreduzzi, A. Aquili, E. De Paola, L.G. Stoica, A. Di Marco, Beamforming Algorithm for Vehicle Cabin Acoustic Comfort Application, in: Proceedings of the 10th Convention of the European Acoustics Association Forum Acusticum 2023, European Acoustics Association, Turin, Italy, 2022: pp. 4559-4566. https://doi.org/10.61782/fa.2023.1091.

[13] J.J. Christensen, J. Hald, Beamforming, Beamforming No. 1 (2004). https://www.bksv.com/media/doc/bv0056.pdf.

[14] M. Garcia-Pedroche, G. Bennett, Aeroacoustic Noise Source Identification Using Irregularly Sampled LDV Measurements Coupled with Beamforming., in: 2011. https://doi.org/10.2514/6.2011-2719.

Copyright © FrancoAngeli.
This work is released under Creative Commons Attribution - Non-Commercial – No Derivatives License.
For terms and conditions of usage please see:
http://creativecommons.org.